Tunable Environment-Enhanced Mid-Infrared Absorber Based on Voltage Modulation

Gongli Xiao, Zifan Lai, Hongyan Yang, Bing Wang, and Haiou Li

Abstract—**In this paper, we propose a design of a mid-infrared Metamaterial Absorber (MIMA). The MIMA is composed of a thin metamaterial nanostructure of period array of cross-circular structure of Ti with continuum graphene layer and bottom film is Al substrate, the middle dielectric layer is a stack of Si_3N_4 and SiO_2. The coupling of surface plasmon resonance (SPR) of graphene, metal Ti and dielectric layers and the intrinsic absorption of the material enhance broadband absorption. The MIMA maintains 97% average absorption in the 3.8∼6.5 μm in the background refractive index of 1.33. MIMA maintains 80% average absorption within an incidence angle of 50 and it is polarization insensitive. Dynamic tuning of the MIMA absorption bandwidth by changing the Fermi energy level of graphene by applying a voltage to the graphene surface. The absorption bandwidth can broaden in complex environments (water, ice, alcohol). The proposed research shows excellent applications in thermal emitter and photocatalysis, infrared camouflage in complex environment.**

Index Terms—**Environment-enhanced, metamaterial absorber, mid-infrared, tunable, voltage.**

I. INTRODUCTION

METAMATERIALS are a class of man-made materials with special properties not found in nature and which have properties that cannot be achieved with conventional materials. Researchers are able to tune their permittivity (ε) and permeability (μ) through physical structure design to achieve new properties that break the limits of natural laws and obtain extraordinary physical properties, quantum information [1], [2], For example, metamaterials can modulate light and electromagnetic waves, because the size of its structure is smaller than the wavelength at which it acts, the special nanostructure of the light-manipulating metamaterial is able to scatter light in a specific way [3], [4]. Metamaterial absorbers (MAs) are

the important application of metamaterials. MAs based on the theory of surface plasma resonance(SPR) gradually be used for solar energy harvesting [5], photoelectric detection [6], sensor [7] etc. Broadband strong absorber is critical for the domain of energy harvest and infrared camouflage. According to the field of application. MAs also can be divided by visible [8], infrared [9] and terahertz absorbers [10].

In 2008, Landy et al. [11] proposed a near-perfect proposed a near-perfect absorber, introducing the concept of MIMA for the first time, which led to subsequent research on metamaterial perfect absorbers. Then with the discovery of new materials, researchers designed MAs based on various MIMs. MAs also can be designed based on 2D materials such as graphene [12], black phosphorus [13],combined structures of graphene and black phosphorus [14].

Graphene is a unique 2D material with only atomic thickness. It has zero bandgap and unique electrical and optical properties that hold promise for a wide range of applications. The surface conductivity can be controlled by doping and tuning that Fermi energy level (E_F) and thus dynamically controlling the SPR [15]. The E_F of graphene can be dynamically tuned by externally applied voltage and chemical doping. Graphene-based plasmonic excitonic resonance can be fabricated with extremely high speed, low drive voltage, low power consumption and compact size for a wide range of applications from visible light to terahertz wavelengths. [16]

Although some MAs have achieved high performance. Such as, Fann et al. [17] designed a metal Ti, dielectric layer of SiO_2, and substrate of metal Al structure for a far-wave mid-infrared (8∼16 μm) broadband perfect absorber, it maintains a broadband absorption of 94% at 8∼13 μm. In 2022 Huang et al. [18] proposed a absorber with random $Au-Al_2O_3-Au-SiO_2$ structure. the MA maintains an absorption of over 90% in the 8.33∼15.09 μm, with an overall average absorption of 95.17%. Most of them only focus on increasing the absorption rate in air. However, improving absorption performance and dynamic tunable absorption bandwidth considering MA in complex environments are very lack. Therefore, the application of MIMA in complex background environments and tune absorption bandwidth of MIMA by voltage have become a new research direction. In recent years, many researches have provided many methods to dynamically tune the absorption bandwidth. Based on the characteristic mode theory, Suo et al. [19] theoretically proposed a flexible transparent absorber with broadband absorption, which can achieve absorption bandwidth extension by inputting current to the resistor on the absorber. In 2022

Gongli Xiao, Zifan Lai, and Haiou Li are with the Guangxi Key Laboratory of Precision Navigation Technology and Application, Guilin University of Electronic Technology, Guilin 541004, China.

Hongyan Yang is with the Guangxi Key Laboratory of Optoelectronic Information Processing, School of Optoelectronic Engineering, Guilin University of Electronic Technology, Guilin 541004, China (e-mail: hyyang@guet.edu.cn).

Bing Wang is with the School of Electronics and Information Technology, Sun Yat-Sen University, Guangzhou 510006, China.
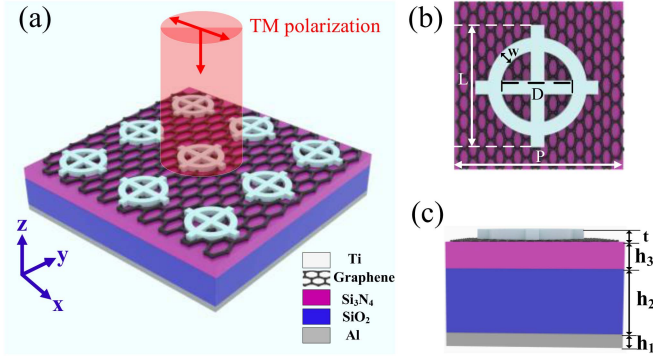
Fig. 1. (a) Schematic diagram of the graphene cross-circular array structure. (b) x-y plane of a single structure, and (c) x-z plane of a single structure.

and 2021, Xiong et al. [20], [21] designed a dual-controlled terahertz bandwidth tunable absorber based on graphene and Dirac semimetals and a dual-tuned bandwidth material absorber based on bulk Dirac semimetals and water, respectively. The above work provides inspiration and ideas for our work, we try to research in the mid-infrared band. It is possible to harvest the thermal energy of mid-infrared wavelength radiation from space [22], [23]. The wavelengths of 3∼8 μm mid-infrared band covers the most important transparent window of the atmospheric infrared (3∼5 μm), where people can perform infrared detection by metamaterial absorbers (MAs) [24]. At the same time, MAs can effectively capture electromagnetic waves radiated by high-temperature objects in this band, which is beneficial for thermal imaging and infrared camouflage.

In this paper, we propose an MIMA that operates in the range of 2.5∼8 μm. In a refractive index of 1.33, it maintains an average absorption of 97% at 3.8∼6.5 μm. Broadband absorption is enhanced by the SPR of graphene, Ti, and dielectric layers with the intrinsic absorption of the material. The absorption bandwidth of MIMA can be dynamically tuned by changing the E_F of graphene and it will expand in complex environments (water, ice, alcohol). It maintains 80% average absorption within an incidence angle of 50 degree and polarization insensitive. It is beneficial for infrared camouflage, thermal emitter, photocatalysis, and infrared detection in complex environments.

II. STRUCTURE AND SIMULATION

The array structure of the MIMA is shown in Fig. 1(a), and its x-z plane and x-y plane views are shown in Fig. 1(b) and (c), the structure is based on an Al substrate of height h_1, the dielectric layer is a joint stack of SiO$_2$ at h_2 height and Si$_3$N$_4$ at h_3 height. Continuous coverage of 2D material graphene on the dielectric layer, and the top layer is a cross-circular structure including P, t, L, W, and D. P is 1600 nm, t is 80 nm, L is 1200 nm, W is 200 nm, D is 600 nm, h_1 is 250 nm, h_2 is 350 nm, h_3 is 200 nm. A 3D FDTD method (Ansys Lumerical Photonics Simulation & Design Software) was used for the simulation, with periodic boundary conditions in the x and y directions and anti-symmetric boundary conditions in the x direction and symmetric boundary conditions in the y direction, and set to PML (Perfect Match Layer) boundary conditions in

the z direction. We set the background environment refractive index to 1.33 to mimic the water environment. A TM polarized plane light source in the wavelengths of 2.5∼8 μm is placed directly above the array structure, reflectance and transmittance monitors are placed above the plane light source and below the structure, respectively, to obtain reflectance and transmittance data.

Although this is a simulation work, we tried to explore the possibility of its fabrication. First, we grow an Al film on the substrate by evaporation through vacuum coating. [25] The chemical vapor deposition (CVD) method is used to deposit a certain thickness of SiO$_2$ by chemical reaction between SiH$_4$ and O$_2$ gases at high temperatures. [26] The gas source was then replaced with silicon source gas and ammonia as reactants in the same way, and Si$_3$N$_4$ was generated on a large scale in high temperature conditions. Then, Graphene layer is uniformly coated on Si$_3$N$_4$ surface using ionic gel. [27] Finally, the patterned Ti is etched using reactive ions on the Ti film based on an anodic aluminum oxide (AAO) template. [28]

The refractive index data of Ti and Al are from Rakic's experimental data [29], SiO$_2$ is from Palik [30], and Si$_3$N$_4$ is from Kischkat [31]. The surface conductivity of graphene can be measured directly [32]. The formula for the conductivity of graphene can be described by the Kubo formula based on the intra band and inter band contribution: [33]

$$\sigma_G = \sigma_{\mathrm{intra}} + \sigma_{\mathrm{inter}}, \tag{1}$$

$$\sigma_{\mathrm{intra}} = i\frac{e^2 K_B T}{\pi \hbar (\omega + {}^i\!/_\tau)}\left[\frac{E_F}{K_B T} + 2\ln\left(e^{-E_F/K_B T} + 1\right)\right], \tag{2}$$

$$\sigma_{\mathrm{inter}} = i\frac{e^2}{4\pi\hbar}\ln\left[\frac{2E_F - (\omega + {}^i\!/_\tau)\hbar}{2E_F + (\omega + {}^i\!/_\tau)\hbar}\right], \tag{3}$$

Where e is the electron charge, $\hbar$ is the reduced Planck's constant, K_B is Boltzmann's constant, T is the temperature in Kelvin, E_F is the fermi level, $\mu = 10000 \ \mathrm{cm}^2/(V \cdot s)$ is the carrier mobility, The relaxation time can be expressed as $\tau = \mu E_F/eV_F^2$, where $V_F = 10^6$ m/s is the Fermi potential. In the infrared wavelength, the surface conductivity can be expressed as a Drude-like model [34].

$$\sigma_G = \frac{ie^2 E_F}{\pi\hbar^2(\omega + {}^i\!/_\tau)}, \tag{4}$$

E_F is the fermi level, e is the electron charge, ω is frequency. $\hbar$ is the reduced Planck's constant. The relaxation time can be expressed a $\tau = \mu E_F/eV_F^2$.

III. RESULTS AND ANALYSIS

Fig. 2(a) shows the absorption spectrum of the MIMA, the result is shown that the high absorption of 97% is maintained in the NIR band from 3.8 μm to 6.5 μm. Absorption can be expressed as A = 1-T-R, where the transmittance T = $|S_{21}|^2$ and the reflectance R = $|S_{11}|^2$. S_{11} and S_{21} are the scattering parameters associated with the reflection and transmission coefficients. the
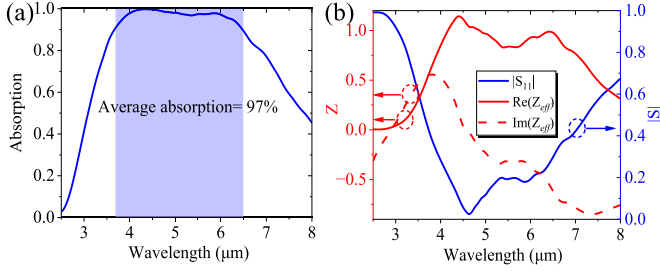
Fig. 2. (a) Absorption spectrum of MIMA; (b) the real and imaginary part of the effective impedance (Z_{eff}) and Reflection coefficient $|S_{11}|$.
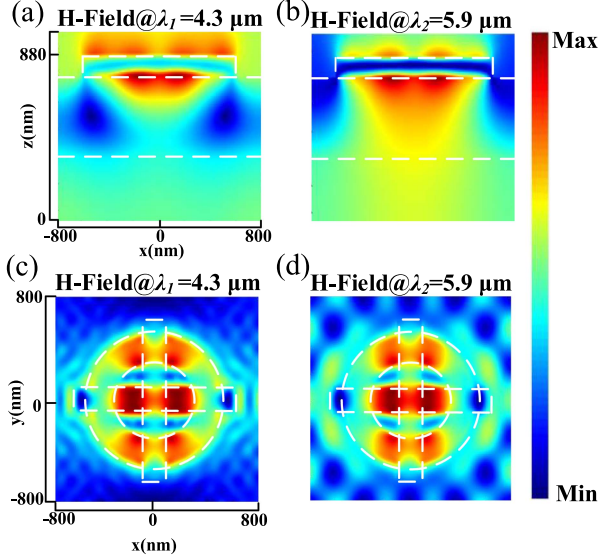

Fig. 3. Magnetic field distribution for the MIMA resonance wavelength of (a) λ_1, (b) λ_2 of x-z plane, and (c) λ_1, (d) λ_2 of x-y plane.

reflection-related S_{11} infinitely tends to zero, so the absorption can be written as A = 1-R = 1-$|S_{11}|^2$.

We calculated the equivalent impedance of the absorber by S-parameter evolution as shown in :

$$Z_{eff} = \sqrt{\frac{(1+S_{11})^2 - S_{21}^2}{(1-S_{11})^2 - S_{21}^2}} \qquad (5)$$

Description of the broadband absorption of MIMA can be explained by impedance matching theory (IMT). Fig. 2(b) shows the real and imaginary part of impedance (Z_{eff}) of MIMA with wavelengths. The Z_{eff} is closer to the intrinsic impedance of the free space in the high absorption region (4~6 μm), while the reflection coefficient is also the lower than other wavelengths. The error stems from not perfect absorption in the wavelengths.

To further investigate the physical mechanisms, Fig. 3(a) and (b) show the magnetic field distribution of the MIMA with graphene layer at resonance wavelength band between λ_1 and λ_2 in Fig. 2. At λ_1, the enhancement of the magnetic field is distributed the upper and the lower of Ti film and the left and right bottom corners of the dielectric layer, it is the characteristics of propagation surface plasmon resonance (PSPR). The effect of the metamaterial geometry parameters of the absorber on the

PSPR can be expressed as:

$$K_{sp} = K_0 \sin\theta + i \cdot \frac{2\pi}{P} \qquad (6)$$

At λ_2, the enhancement of the magnetic field occurs in the cavity of top Ti film and Al bottom film (not significantly enhance), showing the characteristics of local surface plasmon resonance (LSPR). Its resonant behavior can be represented by the LC circuit model [35], its resonance wavelength is expressed as:

$$\lambda = 2\pi\sqrt{LC/2} \qquad (7)$$

$L = L_r + L_b$, L_r is the motion inductance of the resonator and L_b is the motion inductance at the substrate Al. $C = C_e + C_n$, C_e is the capacitance of the neighboring resonators, C_n is the capacitance between the two metal parallel plates. The capacitance of the adjacent resonator PSPR and LSPR combined to result in broadband absorption of the MIMA in detail. At the same time, a larger magnetic field is generated at the center of the cross-circular structure, producing ohmic heat effect and achieving strong absorption in x-y plane, as shown in Fig. 3(c) and (d).

We try to predict the optical response using an equivalent circuit theory (ECT). The metal Ti resonator combined graphene can be described by a series RLC circuit model [36], [37]. Magnetic field enhancement will create current. As a result, the equivalent resistance (R) in the magnetic field enhancement region must be considered when implementing the equivalent LC model. The surface resistance of graphene is R_s and it is connected in parallel with the RLC circuit

$$Z_{FSS} = \left[R - j\left(\frac{1-\omega^2 LC}{\omega C}\right)\right] // R_s \qquad (8)$$

R is the surface resistance of metal Ti. L and C are related to the shape of Ti. The dielectric layer impedance can be expressed as:

$$Z_d = jZ_{d1}\tan(\beta_1 d_1) \qquad (9)$$

Where $Z_{d1} = Z_0/\sqrt{\varepsilon_{r1}}$ and $\beta_1 = k_0\sqrt{\mu_{r1}\varepsilon_{r1}}$, K_0 is free space wave number, $d_1, \varepsilon_{r1}, \mu_{r1}$ are thickness, relative permittivity, relative permeability of dielectric layer respectively. The substrate Al is approximately completely reflecting the electromagnetic wave and is seen as a wire in the circuit model and its impedance $Z_b = 0$. According to the ECT, the total impedance can be expressed as

$$Z_{eff} = \frac{Z_{FSS} \cdot Z_d}{Z_{FSS} + Z_d} \qquad (10)$$

Fig. 4(a) and (b) show schematic of the circuit model and a plot of Z_{FSS} and Z_d complex impedance with wavelengths. $Im(Z_{FSS})$ is closer to zero, $\frac{1}{\omega C}$ is nearly equal to ωL, it is close to impedance matching condition in 4.5~6.5 um. While $Re(Z_{FSS})$ becomes smaller in this wavelength, the surface current becomes larger, producing a stronger absorption in MIMA, which corresponds to the smaller reflection coefficient in Fig. 2(b). The impedance of the Z_d layer can be adjusted by varying the thickness (d) and material to regulate impedance to modulate absorption.
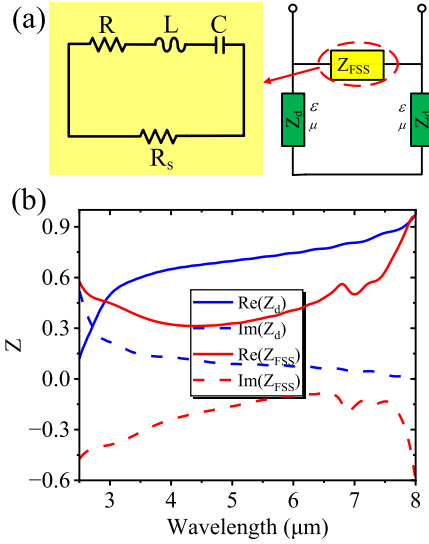
Fig. 4.   (a) MIMA equivalent circuit schematic; (b) The complex impedance of Z_{FSS} and Zd.
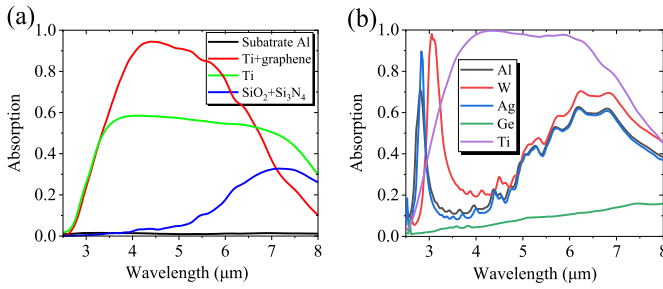

Fig. 5.   (a) MIMA absorption spectrum in four parts (Ti+graphene, Ti, substrate Al, and SiO_2+Si_3N_4); (b) Absorption spectrum of the cross-circular resonator for Al, W, Ag, Ge and Ti.

IV. MATERIAL AND STRUCTURE PROPERTIES

In order to investigate the contribution of the absorption of various parts of MIMA, we divided MIMA into three parts: one part is the top layer (Ti + graphene), one part is the middle dielectric layer (SiO_2+Si_3N_4), and the last part is the bottom Al. And we simulate the absorption of these three parts as shown in Fig. 5(a). red curve is the absorption spectrum of top layer (Ti+graphene), blue curve is the absorption spectrum of middle layer (SiO_2+Si_3N_4), black curve is the absorption spectrum of bottom Al. The top layer occupies the majority absorption of MIMA in 4∼5 μm wavelengths. The result is shown that the combined effect of loss of metal Ti and SPR effect between metal Ti and dielectric layer produces >90% average absorption at 4∼5 μm. It is worth mentioning that it is located in the transparent window of 3∼5 μm atmospheric effective radiation, so it has practical physical application. In the wavelength of 3∼5 μm, infrared radiation has a good match with the thermal radiation of the ground, MIMA can be applied to thermal emitters and photothermal conversion [38], [39]. Middle layer (SiO_2+Si_3N_4) provides a part of absorption in MIMA in 5.5∼8 μm. This is controlled by the intrinsic absorption of the material the refractive index of the imaginary part of Si_3N_4

controls the excitation of the intrinsic absorption of incident light at target wavelengths, and SiO_2 (n = 1.45) can control the resonant bands at target wavelengths [40]. In addition to reflect electromagnetic waves, the substrate Al also dissipates a small portion of electromagnetic waves, this will also cause slight absorption in substrate Al.

Furthermore, we focused on absorption spectrum of the top layer, red curve is the absorption spectrum of the top layer with graphene, green curve is the absorption spectrum of the top layer without graphene. We found that the addition of graphene in top layer can significantly increase the absorption of the MIMA top layer in the environment of water. Graphene has good thermal conductivity, thereby the addition of graphene can enhance SPP between metal Ti and graphene in environment of water and simultaneous excitation of strong thermal effects.

Fig. 5(b) shows the comparison of the effect of different metal materials on the absorption spectrum, the black curve is Al, the red curve is W, the blue curve is Ag, the green curve is metal Ge and the purple curve is Ti. It is shown that the overall average absorption of Ge metal in the NIR band is less than 20%, the plasma resonance is lower. In contrast, for metals Al, W and Ag, they have a narrow absorption peak in the near to mid-infrared band of 1∼3.8 μm. Because W, Ag and Al are high-Q metals, the conductivity deviates increasingly from ideal conditions with wavelengths, and they meet the impedance matching condition only in a small wavelength range. [41] While in the mid-infrared band of 4∼8 μm, they produce broadband absorption peaks with low absorption. This is because different metal materials affect the bandwidth and absorption of MA. It is determined by the inherent dispersion properties of the metal, and Ti is a high loss metal, so the impedance matching condition is satisfied at the appropriate thickness, which then excites the low Q-factor cavity, resulting in superior absorption performance [42].

V. ENVIRONMENT EFFECT

Then, we analyzed the effect of special environment such as real environment, incident angle and polarization angle. Fig. 6(a) illustrates the refractive index data for air (purple), water (blue) [43], ice (green) [44], and alcohol (orange) [45], the solid line represents the real part of the refractive index of the liquid (n) and the dashed line represent the imaginary part of the refractive index of the liquid (k).These parameters are proposed to be close to reality in the simulation. Fig. 6(b) shows the absorption spectrum of MIMA in environment of air (purple solid line), water (blue solid line), ice (green solid line), and alcohol (orange solid line). The result is shown that MIMA exhibits superior performance in various liquid backgrounds compared to air. Absorption bandwidth extends to both sides. It is interesting to note that the average absorption in the 3∼4 μm wavelength is significantly increase when MIMA is placed in a special environment, and it maintains a high average absorption in the 3∼5 μm wavelength range. Mid-Infrared wavelength of 3∼5 μm can transmit through substances such as water and glass, and the 3∼5 μm band is also an important atmospheric infrared radiation window. MIMA is more suitable for 3∼5 μm IR windows in special environment and benefits infrared sensing and detection
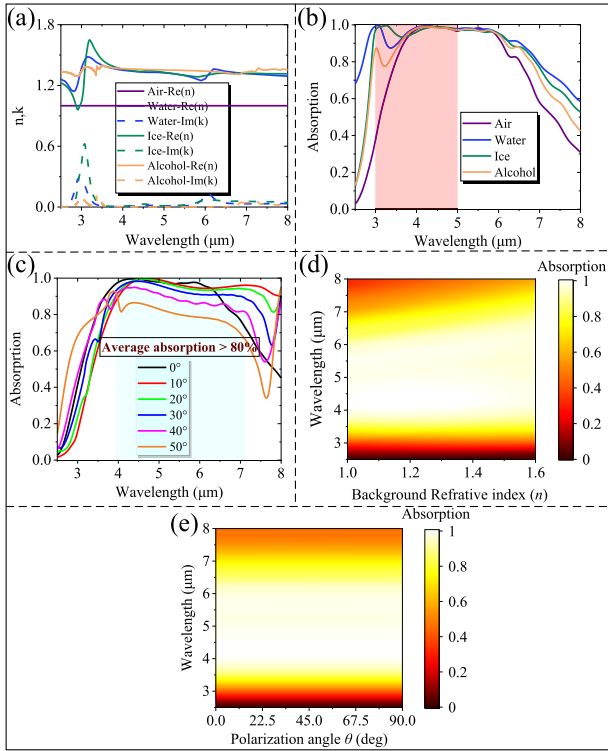
Fig. 6. (a) The spectrum of the real (solid line) and imaginary (dashed line) parts of the refractive index with air, water, ice, and alcohol; (b) MIMA's absorption spectra in different environments, including air, water, ice, and alcohol; (c) the MIMA's incident angle dependence curves; (d) MIMA absorption spectrum in the case of background refractive index (n = 1~1.6); (e) the graph of MIMA absorption spectrum with polarization angle (0~90°).

Fig. 7. (a) the absorption spectrum for varying different E_F from 0.1 to 0.9 eV. (b) the bandwidth with different E_F.

TABLE I
COMPARISON OF INFRARED ABSORBERS WITH OUR WORK IN RECENT YEARS

References	Structure	Maximum Average absorption	Operate wavelength
[46]	Ti-ZnS/Si-Ti	92.1%	8~12 μm
[47]	hBN-CaF$_2$-Au	95%	6.49~7.295 μm
[48]	Ti-Ge-Ti	86%	8.5~12.5 μm
[49]	Cr-SiO$_2$-Ti	90%	1~3.4μm
This work	Ti-graphene-Si$_3$N$_4$-SiO$_2$-Al	98%	3~8 μm

in special environments. The same type of work has been less reported before.

Fig. 6(c) shows the MIMA incident angle dependence curve. As the incident angle increases from 0 to 50°, the absorption bandwidth gradually expands while the average absorption gradually decreases. Overall average absorption remains above 80%. Fig. 6(d) shows absorption spectrum by changing the refractive index of environment changes from 1 to 1.6. As the ambient refractive index increases from 1 to 1.6, the result is show that the absorption bandwidth expands to longer wavelengths while maintaining an average absorption of 97%. The correlation of polarization is due to the symmetry of the shape of the metamaterial and the anisotropy and isotropy of the material conductivity. Because the cross-circular Ti structure is centrosymmetric, the conductivity model of Ti is derived from the Drude model and conductivity is isotropic. The conductivity model of graphene is taken from the Drude-like model and conductivity is also isotropic. Therefore, it is polarization independent as shown in Fig. 6(e).

VI. VOLTAGE MODULATION

Fig. 7(a) shows the absorption spectrum of MIMA when changing the E_F of graphene. As the E_F increases, the bandwidth progressively narrows while remains high average absorption. Due to the dynamic tunable characteristic of Graphene's E_F,
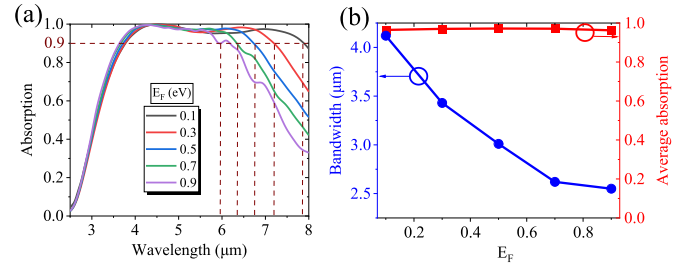
the bandwidth tunability of MIMA is reversible. The Curve of average absorption and Bandwidth with vary of E_F is shown in Fig. 7(b), the absorption bandwidth increases from 2.5 μm to 4.2 μm as the E_F of graphene decreases from 0.9 eV to 0.1 eV, while the average absorption maintains 97%. The usage of ionic gels can reduce the real modulation voltage of graphene. [27] This demonstrate the dynamic tunability of the bandwidth of this MIMA. The behavior of dynamically modifying the bandwidth while maintaining the average absorption in complex environment is special among previous published researches. This provides ideas for dynamically tunable optical devices in background environment.

Finally, we compare our work with other previous mid-infrared absorber work as shown in Table I, our work has the advantage of tunable bandwidth, large bandwidth and high absorption.

VII. CONCLUSION

In conclusion, based on the FDTD method, we proposed an environment-enhanced mid-infrared metamaterial absorber based on the SPR effect and graphene-Ti coupling structure. The proposed MIMA exhibits a nearly perfect average absorption of 97% in the wavelengths of 3.8~6.5 μm in background refractive index of 1.33. Broadband absorption is enhanced by the SPR of graphene, Ti, and dielectric layers, as well as the material's intrinsic absorption. MIMA can enhance the absorption bandwidth in the special background environment (water, ice and alcohol). The bandwidth can also be tuned by changing the E_F of graphene. MIMA maintains 80% average absorption within an incident angle of 50 degree and it is polarization insensitive. The graphene is insoluble in water, Ti and Al are chemically stable, the research results are hopeful for infrared camouflage, infrared detection, thermal emitter and photocatalyst applications.

REFERENCES

[1] P. Markos and C. M. Soukoulis, "Transmission properties and effective electromagnetic parameters of double negative metamaterials," *Opt. Exp.*, vol. 11, no. 7, pp. 649–661, Apr. 2003.

[2] R. B. Greegor, C. G. Parazzoli, K. Li, B. E. C. Koltenbah, and M. Tanielian, "Experimental determination and numerical simulation of the properties of negative index of refraction materials," *Opt. Exp.*, vol. 11, no. 7, pp. 688–695, Apr. 2003.

[3] S. Jahani and Z. Jacob, "All-dielectric metamaterials," *Nature Nanotechnol., Rev.*, vol. 11, no. 1, pp. 23–36, Jan. 2016.

[4] F. Wu, T. T. Liu, and S. Y. Xiao, "Polarization-sensitive photonic bandgaps in hybrid one-dimensional photonic crystals composed of all-dielectric elliptical metamaterials and isotropic dielectrics," *Appl. Opt.*, vol. 62, no. 3, pp. 706–713, Jan. 2023.

[5] K. - T. Lee, C. Ji, and L. J. Guo, "Wide-angle, polarization-independent ultrathin broadband visible absorbers," *Appl. Phys. Lett.*, vol. 108, no. 3, 2016, Art. no. 031107.

[6] W. Li and J. Valentine, "Metamaterial perfect absorber based hot electron photodetection," *Nano Lett.*, vol. 14, no. 6, pp. 3510–3514, Jun. 2014.

[7] J. J. Liu, L. L. Fan, J. F. Ku, and L. L. Mao, "Absorber: A novel terahertz sensor in the application of substance identification," *Opt. Quantum Electron.*, vol. 48, no. 2, Feb. 2016, Art. no. 80.

[8] Y. B. Zhang et al., "Dual band visible metamaterial absorbers based on four identical ring patches," *Physica E-Low-Dimensional Syst. Nanostructures*, vol. 127, no. 6, Mar. 2021, Art. no. 114526.

[9] J. Liu et al., "Ultra-broadband infrared absorbers using iron thin layers," *IEEE Access*, vol. 8, pp. 43407–43412, 2020.

[10] D. Yan and J. Li, "Tuning control of broadband terahertz absorption using designed graphene multilayers," *J. Opt.*, vol. 21, no. 7, 2019, Art. no. 075101.

[11] N. I. Landy, S. Sajuyigbe, J. J. Mock, D. R. Smith, and W. J. Padilla, "Perfect metamaterial absorber," *Phys. Rev. Lett.*, vol. 100, no. 20, May 2008, Art. no. 207402.

[12] S. K. Gupta and P. K. Basu, "Tunability in graphene based metamaterial absorber structures in mid-infrared region," *IEEE Photon. J.*, vol. 14, no. 3, Jun. 2022, Art. no. 2223805.

[13] Y. Li et al., "Dynamically tunable narrowband anisotropic total absorption in monolayer black phosphorus based on critical coupling," *Opt. Exp.*, vol. 29, no. 2, pp. 2909–2919, Jan. 2021.

[14] G. Xiao et al., "Tunable and anisotropic perfect absorber using graphene-black phosphorus nanoblock," *Opt. Exp.*, vol. 30, no. 13, pp. 23198–23207, Jun. 2022.

[15] S. Ogawa, S. Fukushima, and M. Shimatani, "Graphene plasmonics in sensor applications: A review," *Sensors, Rev.*, vol. 20, no. 12, Jun. 2020, Art. no. 3563.

[16] A. N. Grigorenko, M. Polini, and K. S. Novoselov, "Graphene plasmonics," *Nature Photon., Rev.*, vol. 6, no. 11, pp. 749–758, Nov. 2012.

[17] C. H. Fann, J. Zhang, M. ElKabbash, W. R. Donaldson, E. M. Campbell, and C. Guo, "Broadband infrared plasmonic metamaterial absorber with multipronged absorption mechanisms," *Opt. Exp.*, vol. 27, no. 20, pp. 27917–27926, Sep. 2019.

[18] X. Huang, Z. Zhou, M. Cao, R. Li, C. Sun, and X. Li, "Ultra-broadband mid-infrared metamaterial absorber based on multi-sized resonators," *Materials*, vol. 15, no. 15, Aug. 2022, Art. no. 5411.

[19] M. Suo, H. Xiong, X. - K. Li, Q. - F. Liu, and H.-Q. J. R. I. P. Zhang, "A flexible transparent absorber bandwidth expansion design based on characteristic modes," *Results Phys.*, vol. 46, 2023, Art. no. 106265.

[20] H. Xiong, D. Li, and H. Q. Zhang, "Broadband terahertz absorber based on hybrid Dirac semimetal and water," *Opt. Laser Technol.*, vol. 143, no. 8, Nov. 2021, Art. no. 107274.

[21] H. Xiong, Q. Ji, T. Bashir, and F. Yang, "Dual-controlled broadband terahertz absorber based on graphene and Dirac semimetal," *Opt. Exp.*, vol. 28, no. 9, pp. 13884–13894, Apr. 2020.

[22] B. Zhao and Z. M. M. Zhang, "Perfect mid-infrared absorption by hybrid phonon-plasmon polaritons in hBN/metal-grating anisotropic structures," *Int. J. Heat Mass Transfer*, vol. 106, pp. 1025–1034, Mar. 2017.

[23] S. L. Wu, Y. Gu, Y. Ye, H. Ye, and L. S. Chen, "Omnidirectional broadband metasurface absorber operating in visible to near-infrared regime," *Opt. Exp.*, vol. 26, no. 17, pp. 21479–21489, Aug. 2018.

[24] A. Ware et al., "Decoupling absorption and radiative cooling in mid-wave infrared bolometric elements," *Opt. Lett.*, vol. 48, no. 12, pp. 3155–3158, Jun. 2023.

[25] S. Gupta, M. Dixit, M. Baboo, K. Sharma, and N. S. Saxena, "Thickness-dependent mechanical behaviour of aluminium-coated polyethylene terephthalate (PET) films," *Polym.-Plastics Technol. Eng.*, vol. 48, no. 12, pp. 1333–1337, 2009.

[26] K. L. Choy, "Chemical vapour deposition of coatings," *Prog. Mater. Sci.*, vol. 48, no. 2, pp. 57–170, 2003,.

[27] H. Hu et al., "Broadly tunable graphene plasmons using an ion-gel top gate with low control voltage," *Nanoscale*, vol. 7, no. 46, pp. 19493–19500, 2015.

[28] N. Tasaltin, S. Ozturk, N. Kilinc, H. Yuezer, and Z. Z. Ozturk, "Simple fabrication of hexagonally well-ordered AAO template on silicon substrate in two dimensions," *Appl. Phys. a-Mater. Sci. Process.*, vol. 95, no. 3, pp. 781–787, Jun. 2009.

[29] A. D. Rakic, "Algorithm for the determination of intrinsic optical-constants of metal-films: Application to aluminum," *Appl. Opt.*, vol. 34, no. 22, pp. 4755–4767, Aug. 1995.

[30] H. R. Philipp, "Silicon dioxide (glass)," *Handbook of Optical Constants of Solids*, E. D. Palik, Ed., Academic Press, 1997, pp. 749–763.

[31] J. Kischkat et al., "Mid-infrared optical properties of thin films of aluminum oxide, titanium dioxide, silicon dioxide, aluminum nitride, and silicon nitride," *Appl. Opt.*, vol. 51, no. 28, pp. 6789–6798, Oct. 2012.

[32] J. D. Buron et al., "Graphene uniformity conductance mapping (vol 12, pg 5074, 2012)," *Nano Lett., Correction*, vol. 15, no. 1, pp. 803–803, Jan. 2015.

[33] L. A. Falkovsky and A. A. Varlamov, "Space-time dispersion of graphene conductivity," *Eur. Phys. J. B*, vol. 56, no. 4, pp. 281–284, Apr. 2007.

[34] B. Wang, X. Zhang, X. C. Yuan, and J. H. Teng, "Optical coupling of surface plasmons between graphene sheets," *Appl. Phys. Lett.*, vol. 100, no. 13, Mar. 2012, Art. no. 131111.

[35] Y. Q. Ye, Y. Jin, and S. L. He, "Omnidirectional, polarization-insensitive and broadband thin absorber in the terahertz regime," *J. Opt. Soc. Amer. B-Opt. Phys.*, vol. 27, no. 3, pp. 498–504, Mar. 2010.

[36] J. Feng, L. S. Wu, and J. F. Mao, "Switchable broadband/narrowband absorber based on a hybrid metasurface of graphene and metal structures," *Opt. Exp.*, vol. 31, no. 8, pp. 12220–12231, Apr. 2023.

[37] F. Costa, A. Monorchio, and G. Manara, "Analysis and design of ultra thin electromagnetic absorbers comprising resistively loaded high impedance surfaces," *IEEE Trans. Antennas Propag.*, vol. 58, no. 5, pp. 1551–1558, May 2010.

[38] V. K. Malyutenko and S. V. Chyrchyk, "Optically pumped Si emitting device for mid-infrared band," *Proc. SPIE*, vol. 6368, pp. 25–33, 2006.

[39] V. Malyutenko and A. Zinovchuk, "Mid-infrared LEDs versus thermal emitters in IR dynamic scene simulation devices," *Proc. SPIE*, vol. 6368, pp. 97–104, 2006.

[40] Y. Zhou et al., "Ultra-broadband metamaterial absorbers from long to very long infrared regime," *Light Sci. Appl.*, vol. 10, no. 1, Jul. 2021, Art. no. 138.

[41] A. Ghobadi, H. Hajian, B. Butun, and E. Ozbay, "Strong light-matter interaction in lithography-free planar metamaterial perfect absorbers," *ACS Photon.*, vol. 5, no. 11, pp. 4203–4221, Nov. 2018.

[42] L. Zhu, Y. Jin, H. Liu, and Y. Y. Liu, "Ultra-broadband absorber based on metal-insulator-metal four-headed arrow nanostructure," *Plasmonics*, vol. 15, no. 6, pp. 2153–2159, Dec. 2020.

[43] G. M. Hale and M. R. J. A. O. Querry, "Optical constants of water in the 200-nm to 200-micrometer wavelength region," *Appl. Opt.*, vol. 12, pp. 555–563, 1973.

[44] S. G. J. A. O. Warren, "Optical constants of ice from the ultraviolet to the microwave," *Appl. Opt.*, vol. 23, no. 8, 1984, Art. no. 1206.

[45] E. Sani and A. Dell'Oro, "Spectral optical constants of ethanol and isopropanol from ultraviolet to far infrared," *Opt. Mater.*, vol. 60, pp. 137–141, Oct. 2016.

[46] Y. Tang et al., "An infrared metamaterial broadband absorber based on a simple titanium disk with high absorption and a tunable spectral absorption band," *Annalen der Physik*, vol. 532, no. 9, 2020, Art. no. 2000145.

[47] L. Xu, B. Peng, X. Luo, X. Zhai, and L. Wang, "A broadband and polarization-insensitive perfect absorber based on a van der Waals material in the mid-infrared regime," *Results Phys.*, vol. 15, 2019, Art. no. 102687.

[48] X. Y. Shi et al., "Broadband metamaterial absorber based on hybrid multi-mode resonance in mid-wave and long-wave infrared region," *Results Phys.*, vol. 42, no. 7, Nov. 2022, Art. no. 105972.

[49] P. Tang, Z. Q. Liu, Y. Wang, X. S. Liu, P. P. Pan, and G. Q. Liu, "Ultra-wideband midinfrared refractory absorbers," *Opt. Eng.*, vol. 58, no. 11, Nov. 2019, Art. no. 115103.